RESEARCH ARTICLE | APRIL 03 2025

Atomistic simulation of shock compression of bcc molybdenum single crystals: Role of preexisting dislocations and temperature

I. A. Bryukhanov ; E. V. Fomin

J. Appl. Phys. 137, 135901 (2025)
https://doi.org/10.1063/5.0255365

Journal of Applied Physics ARTICLE pubs.aip.org/aip/jap

Atomistic simulation of shock compression of bcc molybdenum single crystals: Role of preexisting dislocations and temperature

Cite as: J. Appl. Phys. **137**, 135901 (2025); doi: 10.1063/5.0255365
Submitted: 29 December 2024 · Accepted: 13 March 2025 ·
Published Online: 3 April 2025

I. A. Bryukhanov[a] and E. V. Fomin

AFFILIATIONS

Institute of Mechanics, Lomonosov Moscow State University, Moscow 119192, Russia

[a]**Author to whom correspondence should be addressed:** ibryukhanov@gmail.com

ABSTRACT

It is known that plastic relaxation behind the shock wave front in metals and alloys is achieved through intense dislocation multiplication. Most of the molecular dynamics simulations usually consider perfect crystals, in which dislocation needs to be nucleated. The present paper presents the molecular dynamic simulations of shock wave loading in [100], [110], and [111] molybdenum crystals of micrometer length, both perfect and with dislocations, over a wide range of temperatures from 300 to 2100 K. The evolution of the shock wave structure and the Hugoniot elastic limit (HEL) is analyzed for the dependence of temperature and the presence of dislocations. It is found that behind the wave front, preexisting dislocation loops, depending on their orientation, could either multiply on their own or serve as the nucleation sources of new screw dislocation segments. The formation of twin bands is also found in [110] and [100] Mo crystals with dislocations as well as in perfect [110] crystals. In Mo crystals with preexisting dislocations, the HEL decays monotonically, and the decay rate weakly depends between [110] and [111] orientations. The HEL decays much slower at the front of the elastic precursor in the [100] crystal; however, the post-spike HEL values decay with the same exponent as for [110] and [111] Mo crystals. The decay exponents are found to be in range between 0.25 and 0.45, which agree with experiments when the shock propagation distance is above 0.2 mm. The HEL decreases slightly with increasing temperature, which is also in accordance with experiments.

I. INTRODUCTION

The description of material behavior under high-strain rate deformation is necessary to solve important applied problems of solid body collision[1,2] and laser processing.[3] The shock waves are generated when the solids collide. In planar impact, the material experiences longitudinal compression behind the shock wave front. When the impact intensity exceeds the Hugoniot elastic limit (HEL), plastic deformation begins to develop behind the front, leading to the formation of an elastic precursor.[4] A set of parameters achievable behind the shock wave is called Hugoniot curve, which is used to extract the equation of state.[4] The evolution of the shock wave structure allows us to study the incipient plastic flow, which develops at high stresses and at the same time at relatively low total longitudinal strains.[4] The elastic precursor decay characterizes the intensity of the plastic flow behind its front. A change in decay exponent over the shock propagation distance may indicate a transition in the mechanisms of plastic deformation in alloys.[5,6]

Many experiments study the response of pure bcc metals, such as Fe,[7] Ta,[8] V,[8] Nb,[9] Mo,[9,10] W,[11] and Cr,[11] to impact loading. A key observation from these studies is that the attenuation of elastic precursor in bcc metals consists of two branches, in which the decay exponent of the first branch is much higher than the decay exponent of the second branch. In the case of Mo, the elastic precursor decreases rapidly over the propagation distance smaller than 0.2 mm with the exponent around 0.8–1.0, before transitioning to a slower decay with an exponent of 0.2–0.4.[9,10] It remains an open question whether a relationship can be established between the mechanisms of plastic deformation and the exponent of elastic precursor decay. Recently, in molecular dynamics simulations, we discovered that when dislocation motion is altered by the presence of a solid solution, preventing dislocations from freely overcoming

obstacles, the elastic precursor in copper crystal attenuates more slowly, resulting in a decrease in the decay exponent.[12]

Another result of shock wave experiments is the decrease in HEL with increasing temperature for bcc metals, which distinguishes them from fcc metals, where an increase in HEL with temperature is observed.[13,14] The reason is believed to be due to the weak influence of temperature on the mobility of dislocations in the phonon friction regime, which is shown in atomistic simulations.[15–18] At low stresses, a screw dislocation moves due to the thermally activated nucleation and propagation of the kink pairs. However, at high stresses, one observes transition to the athermal linear regime.[16,18,19] Continuum models using the mobility law of single dislocations show good agreement with experiments on the temperature-dependent HEL decay for many bcc metals, confirming their thermal softening.[16,20]

While there are many results on the shock behavior of bcc metals and crystals,[10,21–26] the most complete information on the processes occurring behind the shock front can only be obtained by explicit modeling of plastic deformation processes. Models of crystal plasticity as well as methods of discrete dislocation dynamics should assume some laws of dislocation evolution, their reactions among themselves and interactions. In this respect, the molecular dynamic simulations, despite their strong limitations on the dimension of system, are perhaps the only possibility to observe the development of plastic deformation processes behind the wave front naturally from the atomic motion.

The atomic models of perfect crystals, in which there are no lattice defects, are quite idealistic because in real crystals there is a certain density of dislocations, even after annealing. In perfect fcc crystals, there are no dislocations in the elastic precursor region. Depending on the shock velocity and temperature, the elastic precursor may exhibit both weak oscillations and larger-scale perturbations caused by dislocation nucleation processes near the plastic wave[27] or the so-called "elastic-plastic collapse."[28–30] The HEL value does not decay but can fluctuate due to these perturbations. The HEL value for perfect crystals can, thus, be a parameter dependent on impact velocity, or particle velocity, and temperature.[27,28] The HEL dependencies on temperature and particle velocity in the shock wave for [110] and [111] copper crystals have been recently obtained.[27]

The molecular simulation of Ta[31–34] and Mo[35,36] perfect crystals identifies the structure of the shock wave. In ⟨110⟩ Mo perfect single crystals, the elastic precursor overshoots the shear stress, after which dislocations on a specific group of slip planes are nucleated.[35] It is shown that the HEL for the [110] and [111] Mo crystals is close when the shock passes 160 nm at the particle velocity of 1000 ms^{-1}, but the [111] crystal has a much larger plateau of elastic precursor.[36] The simulations also found the {112}⟨111⟩ twinning reactions behind the shock front in Mo,[36,37] which have also been observed in earlier experiments[38,39] through postmortem analysis of shocked Mo.

Recently, molecular dynamics simulations are applied to study the behavior of single crystals in which there is already some density of preexisting dislocations.[27,40–45] In these models, the multiplication of preexisting dislocations occurs at much lower stresses than homogeneous dislocation nucleation. Although these stresses are still higher than those observed in the experiment, these models seem to be more realistic providing some qualitative agreement with experiments.[27,41] Such simulations with preexisting dislocations, coupled with the mobility of individual dislocations, allow us to improve and develop models of crystal plasticity.[45–47]

Unlike perfect crystals, the dynamics of preexisting dislocations behind the wave front and the associated shock wave structure in bcc crystals is scarcely studied at the atomistic level. Although the effect of temperature on HEL has been investigated experimentally and theoretically for various bcc metals,[16,20] it is not shown from the direct simulation of dislocation dynamics behind the shock front. The most obvious problem is related to finding the temperature dependence of HEL in crystals with some density of preexisting dislocations. It is interesting to establish whether in atomic models anomalous hardening can be observed, which took place in fcc copper,[27] because the mobility of edge dislocations in bcc metals still tends to decrease with temperature.[16,17] The decay exponent, derived from dislocation dynamics behind the shock wave front, is another feature that can be directly extracted from molecular dynamics and compared with experiments to provide insights into the mechanisms of plastic deformation behind the shock wave front.[27]

In this paper, we aim to study shock compression of Mo single crystals with and without preexisting dislocations in a wide range of temperatures. To analyze the evolution of the shock structure in more detail, we consider crystals with a size on the order of 1 μm along the shock axis. We intend to find the mechanisms of plastic deformation in both ideal crystals and when crystals already have dislocations. We analyze the temperature dependence of the HEL stress and the role of preexisting dislocations on the HEL value and decay. We relate the HEL decay exponent to the identified mechanisms of plastic deformation behind its front and interpret experimental results.

II. METHODS

The Mo single crystals of three different orientations [100], [110], and [111] are created with a close dimensions around $850 \times 28 \times 28\,nm^3$ (Fig. 1). The dislocations are introduced to the crystals by cutting an equal number of vacancy dislocations loops on four different {111} planes. The dislocations have a hexagonal form, which is the most stable on (111) planes,[48,49] and have been used in many previous works.[40,47,50] The dislocation loops of approximately 6 nm diameter are uniformly distributed along the crystals and in the same way for crystals of different orientations (Fig. 1).

In order to transform the initial cuts into dislocations, we slightly shift the atomic layers perpendicular to the cut toward the cut. This is similar to uniaxial compression and release procedure that has been used for vacancy dislocation loop relaxation in tungsten.[50]

First, the fully periodic crystals with dislocations are relaxed at 300 K in an NPT ensemble with zero pressure. To obtain crystal models with similar dislocation spatial arrangement at higher temperatures, we heat the obtained models from 300 K to the desired temperatures of 700, 1100, 1600, and 2100 K. The dislocations are extracted from atomic models using a dislocation extraction algorithm (DXA).[51,52] The obtained dislocation loops in the Mo crystals are mostly ⟨100⟩ and 1/2⟨111⟩ loops that are composed of edge dislocation segments (Fig. 1). Though most of the cuts are transformed into dislocation segments, some of them are not transformed, and

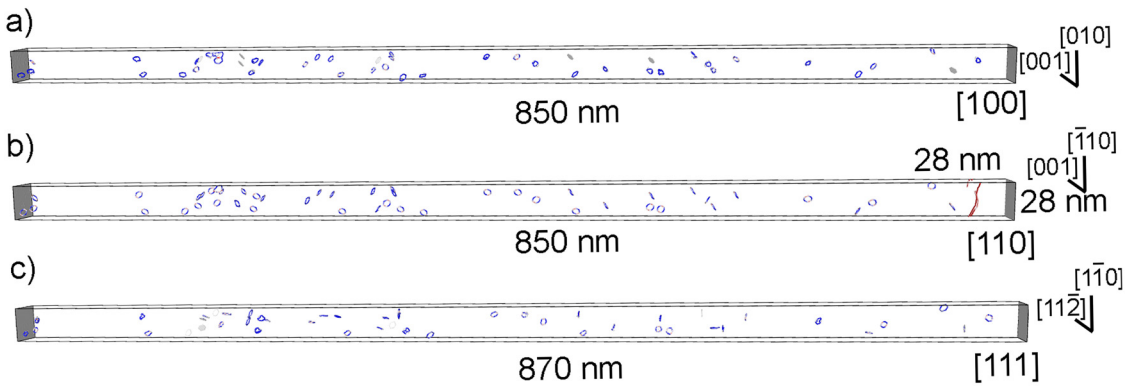

FIG. 1. Molybdenum single crystals oriented along (a) [100], (b) [110], and (c) [111] direction with a preexisting dislocation network. Blue and red lines represent edge and screw dislocation segments. Gray color shows the initial cuts that did not transform into dislocations.

they are not detected by the dislocation extraction algorithm and are represented as a defect mesh in OVITO software.[53]

The dislocation density in [100], [110], and [111] crystals is around $1.2 \times 10^{15}\ \mathrm{m}^{-1}$, respectively, at 300 K and does not change during heating. After relaxation, we remove the periodicity along the shock direction and relax them in the NPT ensemble with zero lateral normal stresses at desired temperature.

The shock compression is applied by assigning constant velocity to the atoms in a 0.8 nm slab from the one end of a crystal with a velocity of 500 and 900 ms^{-1}. For perfect crystals, the velocity is considered in the range between 1000 and 1300 ms^{-1}, for which the previous study[36] with Zhou's potential[54] showed the nucleation of dislocations behind the shock wave. Integration of atomic motion is done in the NVE ensemble with a time step of 1 fs.[27] The simulation time is usually around 120–150 ps. The molecular dynamics calculations are performed using the LAMMPS software[55] with Kokkos GPU acceleration (double precision).[56]

The values of the stress tensor components, temperature, and particle velocity are averaged in bins of 1 nm along the shock direction. The resolved shear stress acting at the primary glide system $\langle 111\rangle\{110\}$ is calculated for [100] and [111] Mo crystals using the following expressions:

$$\tau_{[100]} = \frac{1}{\sqrt{6}}(\sigma_{xx} - \sigma_{yy}), \tag{1}$$

$$\tau_{[111]} = \frac{1}{3}\sqrt{\frac{2}{3}}(\sigma_{xx} - \sigma_{yy}), \tag{2}$$

which are derived using the transformation of the stress tensor to a coordinate system associated with the slip system $\langle 111\rangle\{110\}$, considering the symmetry of the stress tensor $\sigma_{yy} = \sigma_{zz}$.[12] In the case of a [110] crystal, where $\sigma_{yy} \neq \sigma_{zz}$, there are two different expressions for the resolved shear stress at the primary glide systems, namely, in-plane and out-of-plane,[35]

$$\tau^{\mathrm{out}}_{[110]} = \frac{1}{\sqrt{6}}(\sigma_{xx} - \sigma_{zz}), \tag{3}$$

$$\tau^{\mathrm{in}}_{[110]} = \frac{1}{\sqrt{6}}|\sigma_{zz} - \sigma_{yy}|. \tag{4}$$

The embedded-atom method (EAM) interatomic potential with a parameterization proposed by Zhou *et al.* is used to describe the interaction between Mo atoms.[54] The potential is chosen because of its simplicity, which allows a larger number of atoms to be considered in the simulation of shock compression. The potential[54] correctly predicts the thermal softening of the elastic constants c_{11}, c_{12}, and c_{44} compared to experiments[59,60] (Fig. 2), which is important for the present study. Another well-known EAM potential proposed by Ackland[57] predicts much stronger thermal softening (Fig. 2), though it is utilized in many studies such as the edge dislocation

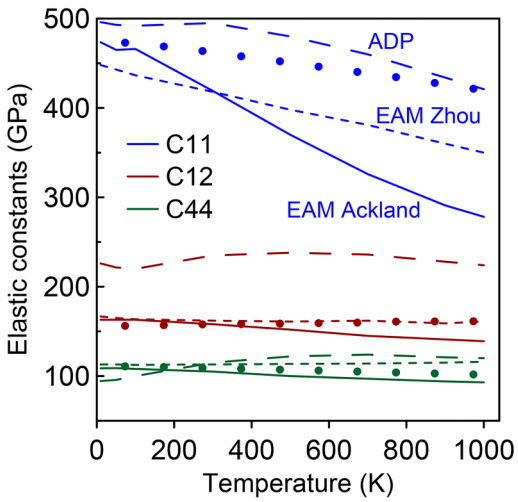

FIG. 2. Temperature dependence of elastic constants c_{11} (blue), c_{12} (red), and c_{44} (green) calculated using Ackland's EAM[57] (line), Zhou's EAM[54] (dashed), and ADP[58] (long dashed) interatomic potentials for Mo. Points refer to experimental data.[59]

mobility[18] and the shear stress relaxation in the [110] Mo crystal.[35] Zhou's potential[54] also shows a good correspondence for the Hugoniot curve with experiments below 200 GPa and has been used recently in the study of shock compression of Mo perfect crystals.[36] The recently proposed ADP potential[58] provides a better description of the dislocation core compared to EAM potentials[54,57] but at the same time predicts much higher value of c_{12} elastic constant than in the experiment (red long dashed line in Fig. 2). Additional simulations are performed using Ackland's potential[57] to verify results obtained (SEM; Figs. S1, S2 in the supplementary material).

III. RESULTS

A. Shock wave structure in perfect crystals

In perfect crystals, after the nucleation of dislocations, which occurs at an initial moment of time at some particle velocity, an elastic precursor is formed and begins to move away from the plastic wave. The plastic deformation picture differs from crystals with dislocations in that there are no dislocations in the elastic precursor and the onset of plasticity occurs only at the front of the plastic wave. Since there are no dislocations in the elastic precursor, it almost does not decay. In the vicinity of the plastic wave near the existing dislocations nucleated, the perfect crystal is compressed above a certain critical value, resulting in the nucleation of new dislocations in this region and their subsequent multiplication and merging with the main front of the plastic wave. This process generates stress relaxation near the plastic wave and produces two rarefaction waves traveling along the elastic precursor front in one direction and in the opposite direction of the plastic wave.[27,29] At moderate impact velocities and temperatures, this nucleation process is localized near the plastic wave and the amplitude of stress relaxation is small, so the elastic precursor is a plateau with small oscillations. However, at higher temperatures, stronger stress relaxation and elastic wave dynamics in the elastic precursor can be observed. Below, we show in more detail these features of the evolution of the shock wave structure in crystals of different orientations. The mechanisms of plastic deformation in perfect crystals differ depending on the crystal orientation.

1. [110] crystal

The characteristic pattern of plastic deformation is illustrated using the example of a particle velocity of 1000 ms^{-1}, which is close to the velocity at which the nucleation of dislocations in a [110] crystal is observed.[36] Figure 3 shows that in the [110] crystal the plastic deformation behind the wave front is attained mainly due to nucleation and multiplication of screw dislocations and the formation of {112} twin bands. At first 60 ps, the elastic precursor front does not contain dislocations [Fig. 3(b)]. The out-of-plane shear stress $\tau^{out}_{[110]}$ [orange curve in Fig. 3(a)] increases during the elastic precursor and then quickly relaxes. The in-plane shear stress $\tau^{in}_{[110]}$ [purple curve in Fig. 3(a)] increases only when the elastic precursor begins its transition to the plastic wave. The $\tau^{in}_{[110]}$ decreases at the top of the plastic wave, when the stress remains constant. Behind the plastic wave front, one can see the formation of twin

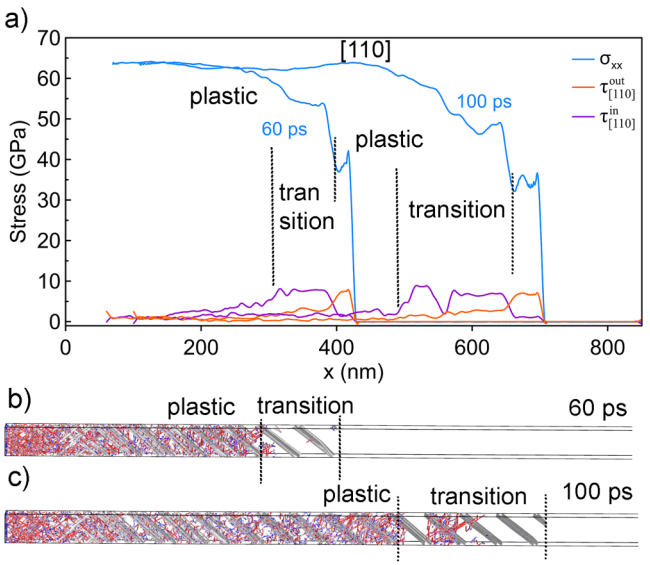

FIG. 3. (a) Shock wave profile in the [110] Mo perfect single crystal at 700 K and particle velocity of 1000 ms^{-1}. The longitudinal stress σ_{xx} and the shear stresses $\tau^{out}_{[110]}$ and $\tau^{in}_{[110]}$ at glide systems ⟨111⟩{110} are shown. Dislocation substructure in the system at (b) 60 and (c) 100 ps. Red lines show the screw dislocation segments, and gray color shows the regions with defective mesh.

bands, which become less pronounced as one moves away from the front. It is noteworthy that inside the twin bands the material has a bcc structure.

As the wave propagates, the elastic precursor moves away from the plastic wave. The transition zone between the elastic precursor and the plastic wave ["transition" in Fig. 3(c)] contains the twin bands and almost free of dislocations. The front part of the elastic precursor is free of lattice defects. The presence of a defect-free elastic precursor, followed by a region that begins with a jump from the elastic precursor and then transitions into a plastic wave, is associated with the in-plane and out-of-plane shear stresses, which become nonzero in these regions, respectively. The resolved shear stress values $\tau^{out}_{[110]}$ and $\tau^{in}_{[110]}$ that reach their maximum in the shock wave are close to each other and about 7 GPa. This value is lower than the critical shear stress for dislocation nucleation at ⟨111⟩{110} slip systems, which is around 17 GPa.[61,62] The reason is the high resolved shear stress in the twin system ⟨111⟩ {112}, which has a higher factor of $\sqrt{2}/3$ compared to $1/\sqrt{6}$ the ⟨111⟩ {110} slip systems [Eqs. (3) and (4)]. The shear stresses in the elastic precursor at the ⟨111⟩ {112} system should promote the propagation of existing {112} twin bands, and their values should be smaller than the twin nucleation stress. In the [110] crystal, the shear stress of 8 GPa is sufficient to sustain the motion of the twin band.

When the particle velocity increases to 1200 ms^{-1}, the plastic deformation mechanisms remain similar. The number of activated slip planes may increase to two when the particle velocity increases. The formation of slip bands has also been observed in previous simulations.[36]

2. [111] crystal

Figure 4(a) shows that at impact velocity of 1300 ms^{-1} and 300 K, a plateau of elastic precursor is observed, where the dislocation are only present in the plastic shock wave [Fig. 4(b)]. The shear stress τ_{111} in the elastic precursor is around 18 GPa, which is close to the ideal shear stress in the ⟨111⟩ {110} slip system.

When the initial temperature increases to 1100 K, the perturbation of the elastic precursor structure is observed in Fig. 4(c). The dislocations still remains only in the plastic wave [Fig. 4(d)], and their substructure is close to the one at 300 K [Fig. 4(b)]. The processes of stress relaxation just near the plastic wave lead to the formation of wave-like structure with rarefaction wave fronts traveling to the front of the elastic precursor. The rarefaction waves are catching up with the compression wave ahead, and the compression waves, on the other hand, overtake the rarefaction waves ahead. Therefore, the observed wave structure evolves with time, according to the laws of propagation of elastic waves. With further increase in temperature, the wave structure in [111] perfect crystals is observed to be similar to that shown in Fig. 4(c) for temperature of 1100 K.

The prerequisites for the appearance of such a structure with increasing temperature are the possibility of easier formation of dislocations at some distance from the plastic wave as a result of the transition of the material from the subcritical state of compression.[29] In this case, the nucleation of dislocations occurs at a more distant distance than at lower temperatures; as a result, they have time to travel some distance, significantly relaxing the stress in this region. Such perturbation was recently observed in molecular dynamics simulation of shock compression of the [111] copper crystal with increased initial temperatures.[27]

B. Hugoniot elastic limit in perfect crystals

The magnitude of the elastic precursor can be calculated by averaging its values between compression-induced oscillations near the plastic wave. Figure 5 shows the HEL dependencies for the Mo perfect crystals. It can be seen that in all crystals the HEL reaches an approximately constant value when the wave passes 200–300 nm.

The HEL becomes almost independent of temperature in the [110] crystal, when the shock wave passes sufficient distance [Fig. 5(a)]. The HEL value decreases with temperature for [111] crystals [Fig. 5(b)]. The higher sensitivity of HEL to temperature is observed for [111] crystals compared to [110] crystals. The HEL value is a characteristic of stress relaxation from the overcritical elastic state near the plastic wave. The decrease in HEL with temperature means that the plasticity mechanisms are thermally activated and are associated with the nucleation of dislocations or the phase transition. Instead, the stress required for the propagation of an existing twin band in the elastic precursor may not significantly depend on temperature (Fig. 3).

The HEL values for the [110] crystal are much lower than for the [111] crystals and close particle velocities of 1000 and 1300 ms^{-1}. This result is qualitatively supported by the experimental

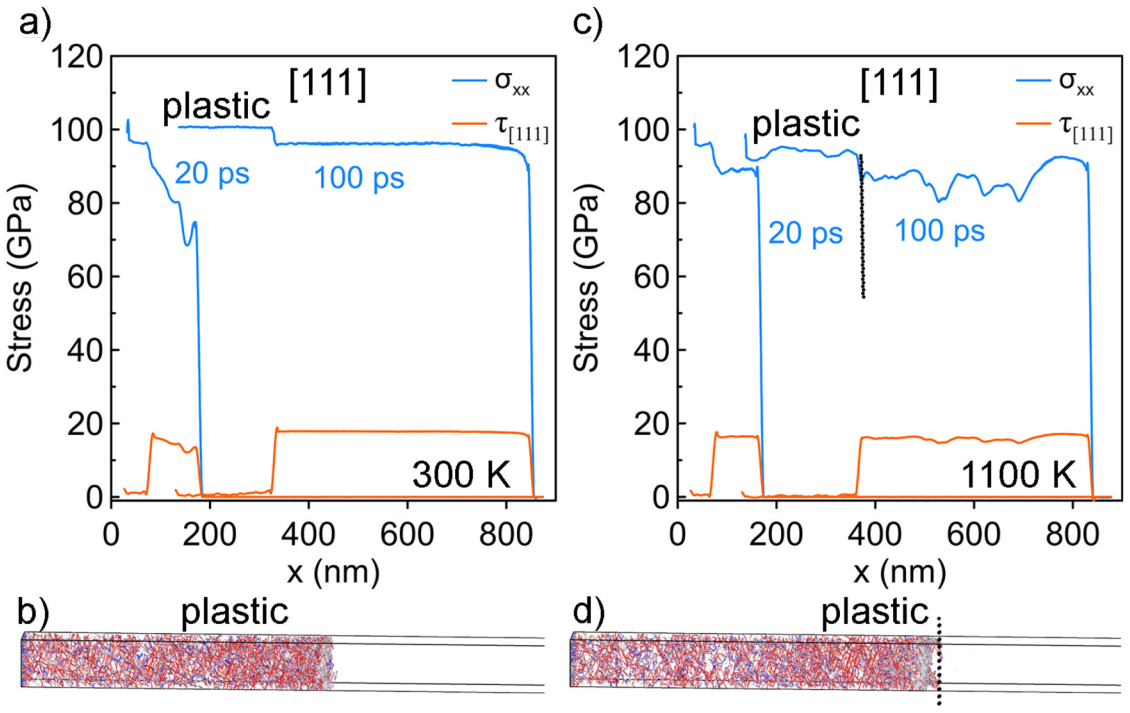

FIG. 4. Shock wave profile in the [111] Mo perfect single crystal particle velocity of 1300 ms^{-1} and temperatures of (a) 300 and (c) 1100 K. Dislocation lines are shown in the plastic waves for (b) 300 and (d) 1100 K.

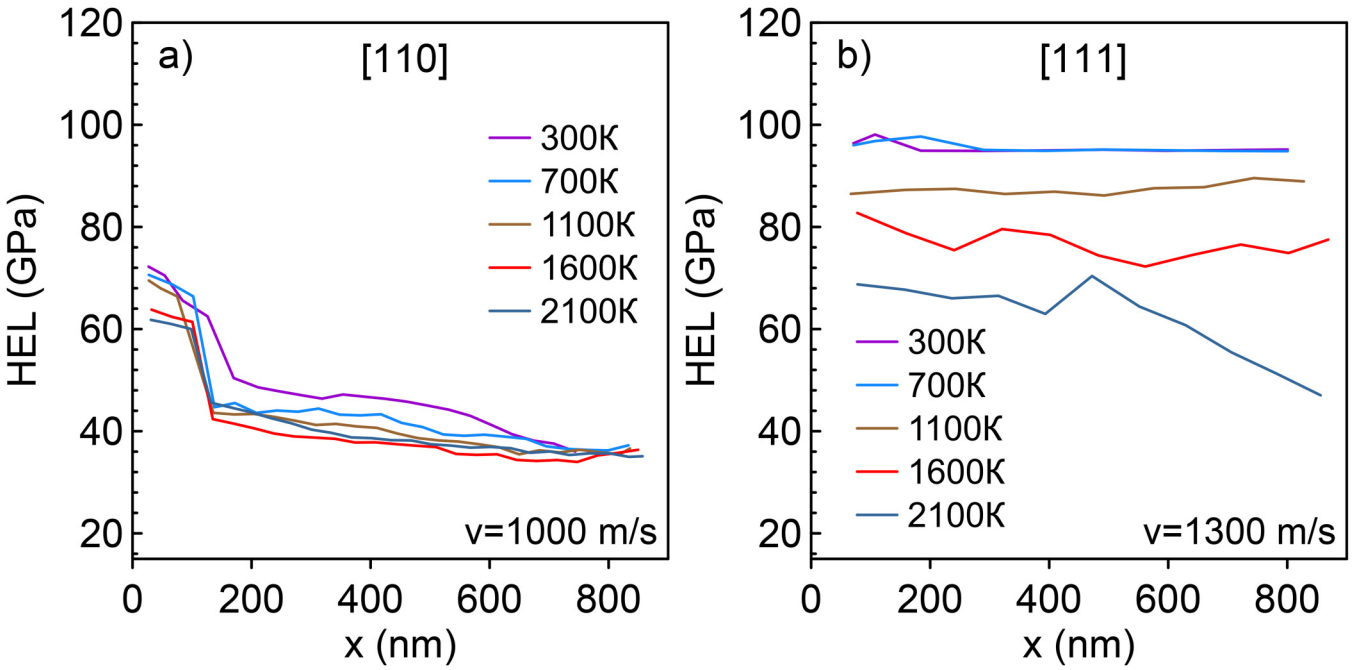

FIG. 5. The dependence of longitudinal stress σ_{xx} at HEL on shock wave propagation distance in (a) [110] and (b) [111] Mo crystals at particle velocities of 1000 and 1300 ms^{-1}, respectively.

data, in which the highest HEL is achieved for [111] crystals, and the HELs for [100] and [110] crystals are close.[23,24] The obtained HEL values for perfect crystals are order of magnitude higher than experimental ones, which are in the range of 4–10 GPa at 2 mm distance.[24] This is typical for molecular dynamic simulation of shock compression and means that the nucleation of dislocations near the plastic wave alone is not the only mechanism of plastic deformation in Mo crystals behind the wave front.

C. Plastic deformation behind shock front in Mo crystals with dislocations

Figures 6 and 7 show the dislocation evolution behind the shock wave in [110] and [111] Mo crystals at 500 ms^{-1}. At this impact velocity behind the wave front, dislocation multiplication is observed, but not so intense as to fill the entire volume of the crystal. The main mechanisms of the plastic deformation in the Mo crystals are associated with the multiplication of screw dislocation segments (red lines in Fig. 6). The directions of the normal to dislocation loops may be calculated as the cross product $\vec{v} \times \vec{b}$ between the direction of the edge segment in the loop $\vec{v}$ and the Burgers vector $\vec{b}$. Under the action of the stress, the preexisting dislocation loops become a source of active dislocations. The analysis of the normal direction shows that the dislocation loops are mostly on the (110) and (112) planes with elongated screw dislocation segments along the corresponding <111> directions. The proportion of normal directions is almost equal between (110) and (112) directions. As the stress behind the wave front relaxes, the dislocation loops elongate due to the motion of screw dislocation segments, both toward and against the shock wave direction. Dislocation loops also cross the periodic boundary of the computational domain and continue their propagation further.

The screw dislocations propagate over larger distances in the [110] crystal than in the [111] crystal, filling more space along the shock axis (Fig. 6). This is because the inclination angle of the screw dislocation lines <111> in the [111] crystal is 70.5° to the direction of the shock axis, which is much closer to the perpendicular direction compared to the inclination angle of screw dislocations 35.3° in the [110] crystal. Therefore, dislocation propagates a further distance in the [110] crystal, and therefore, a smoother shear stress relaxation profile is expected behind the shock wave.

Figure 8 shows that with an increase in temperature and the particle velocity, the similar twin bands can form behind the shock front as in the case of the [110] perfect crystal. The density of twins is higher at the early stages of shock wave propagation due to the higher stress behind. As the shock propagates, the density of twin bands decreases as can be observed in the elastic precursor region and at the top of the plastic wave in Fig. 8.

D. Details of dislocation evolution

As noted earlier, the preexisting dislocation loops have either ⟨100⟩ or 1/2⟨111⟩ Burgers vector. The mechanism of the loops evolution for particle velocities of 500 ms^{-1} depends on their Burgers vector. Figures 9(a) and 9(b) show that when the shock front passes through the 1/2⟨111⟩ loops, the loops rotate to the Burgers vector.

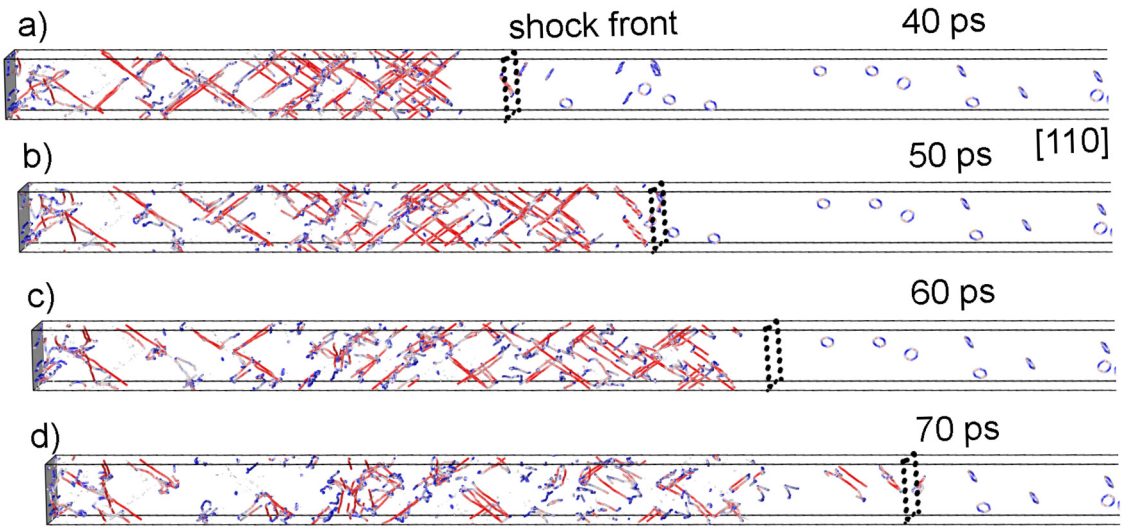

FIG. 6. Shock wave propagation in the [110] Mo single crystal with a preexisting dislocation network at (a) 40, (b) 50, (c) 60, and (d) 70 ps at 500 ms^{-1}. Red and blue lines correspond to screw and edge dislocation segments, respectively. Only the part of the crystal in which there is a shock front is shown.

Thus, the edge segments of the dislocation loop perpendicular to the Burgers vector become screw after rotation. Then, the dislocation loops begin to expand along the Burgers vector. The rotation time is approximately 1–2 ps from 46 to 48 ps in Fig. 9. The shape of the dislocation loop during motion is in many cases not completely elliptical, elongated by screw segments. Some irregularities of the loop shape is observed, in which the screw segments are separated by regions of edge segments [green loops on the left in Fig. 9(c)].

Unlike the $1/2\langle 111\rangle$ loops, the $\langle 100\rangle$ dislocation loops do not rotate as the shock wave passes through them but serve themselves as the sources of new screw dislocation segments [Figs. 9(c)–9(e)]. The evolution of the $\langle 100\rangle$ loops may differ from their orientation to the shock direction as well as from the stress at the elastic precursor wave front. The nucleation of four dislocation screw segments can be observed for the loop at the top of Figs. 9(d)–9(e). The two segments with Burgers vector of $1/2\langle 1\bar{1}\bar{1}\rangle$ and $1/2\langle 1\bar{1}1\rangle$

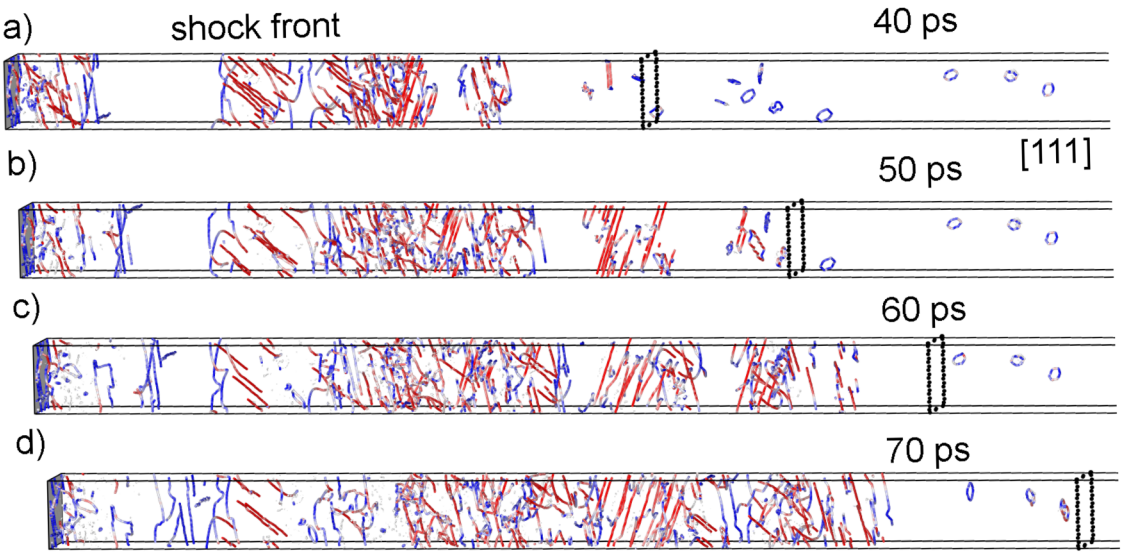

FIG. 7. Shock wave propagation in the [111] Mo single crystal with a preexisting dislocation network at (a) 40, (b) 50, (c) 60, and (d) 70 ps at 500 ms^{-1}. Red and blue lines correspond to screw and edge dislocation segments, respectively. Only the part of the crystal in which there is a shock front is shown.

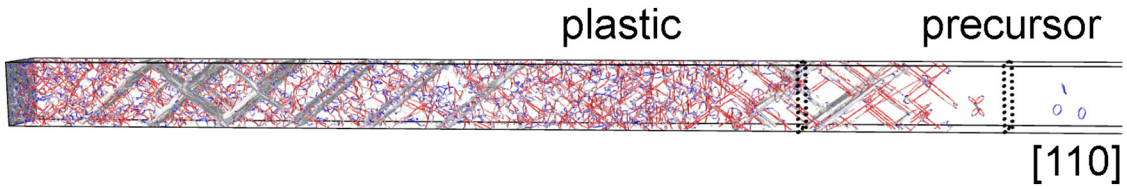

FIG. 8. Twin bands formation during the shock wave propagation in the [110] Mo single crystal with a preexisting dislocation network at 1600 K and 900 ms^{-1}. Red and blue lines correspond to screw and edge dislocation segments, respectively.

propagate along the shock wave direction and the other two ($1/2\langle\bar{1}11\rangle$ and $1/2\langle\bar{1}1\bar{1}\rangle$) propagate in the opposite direction. Also, one can see the nucleation of only two screw dislocation segments, propagating in the opposite directions for the loop in the middle of Fig. 9(e). In the latter case, the $\langle 100\rangle$ loop transforms to a $1/2\langle 111\rangle$ dislocation loop but with the second $1/2\langle 111\rangle$ loop inside.

Figure 10 shows that after the nucleated screw segments propagate some distance from the $\langle 100\rangle$ loop in the [111] Mo crystal, the $\langle 100\rangle$ loop may transform into a $1/2\langle 111\rangle$ loop. A similar transition from immobile $\langle 100\rangle$ loops to mobile $1/2\langle 111\rangle$ loops is observed in [100] Mo crystals.

E. Shock wave structure in crystals with dislocations

The shock wave profiles corresponding to the dislocation evolution figures are shown in Fig. 11. From the very beginning of the shock wave propagation, an elastic precursor is formed, and the shear stress τ behind the wave front relaxes. The appearance and multiplication of screw dislocations at the front of an elastic precursor lead to a decrease in the longitudinal and shear stress at its front. The amplitude of shear stress τ is close between [110] and [111] Mo crystals at submicrometer shock propagation distances, with values between 5 and 6 GPa (Fig. 11). It can also be seen that the plastic wave rise time is higher in the [111] crystal than in the [110] crystal, which is in qualitative agreement with the shock experiment at shock pressure of 12.5 GPa.[23]

The shear stress decreases much smoother behind the shock wave in the [110] crystals than in the [111] one due to a large distance traveled by screw dislocations (Sec. III C). The region of elastic precursor generally contains much less dislocations than in the plastic wave (Fig. 8). It can be seen from Figs. 11(b) and 11(d) that the shear stress in the region of elastic precursor fluctuates near some value, reminiscent of the case of a perfect crystal (Fig. 4). The higher amplitude of fluctuations for the [111] crystal is a consequence of a more localized motion of dislocations. The presence of such region means that the processes of dislocation multiplication are not so intensive that they have time to reduce the shear stress at a shear

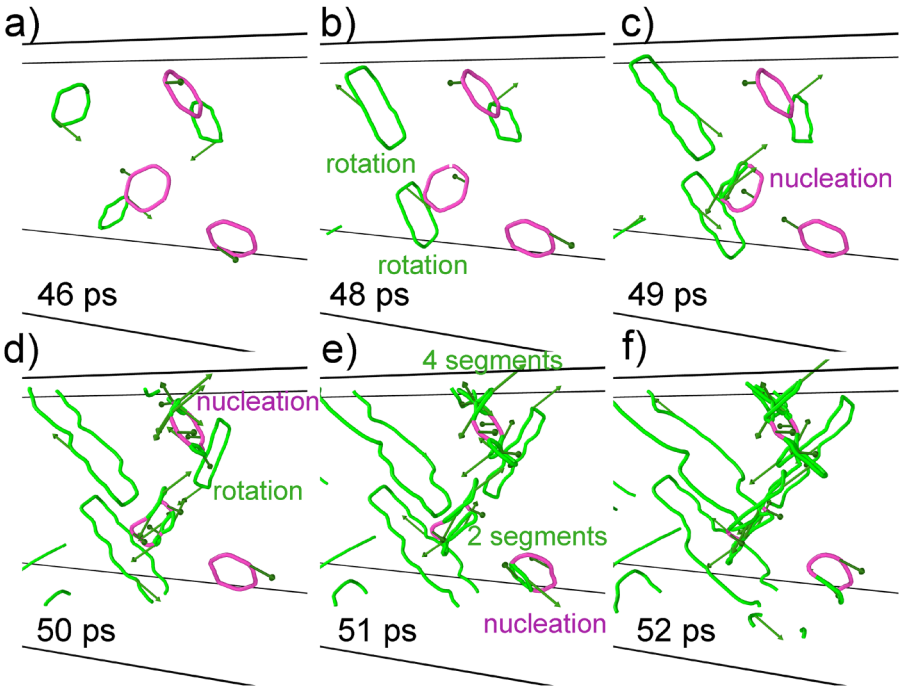

FIG. 9. The evolution of vacancy dislocation loops during the shock wave compression in the [110] Mo crystal at 500 ms^{-1} and 300 K at (a) 46, (b) 48, (c) 49, (d) 50, (e) 51, and (f) 52 ps. Purple and green lines represent $\langle 100\rangle$ and $1/2\langle 111\rangle$ dislocation segments, respectively. Arrows show the direction of the Burgers vector.

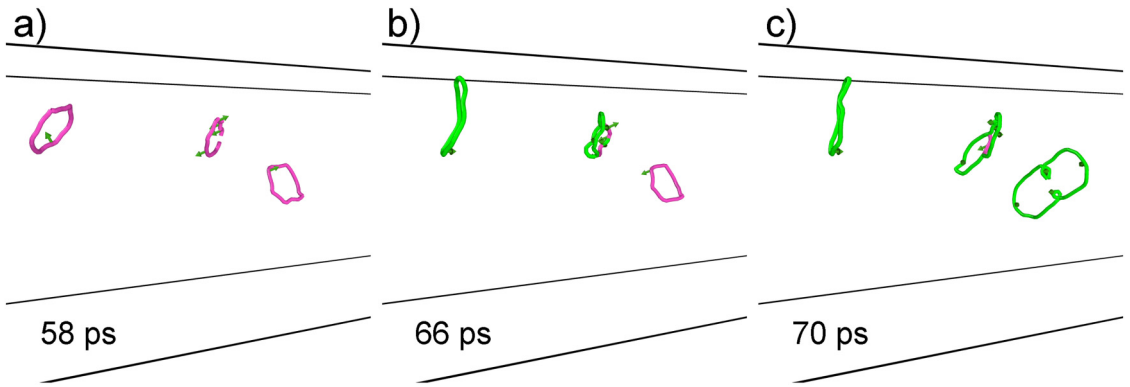

FIG. 10. The transformation of ⟨100⟩ dislocation loops into 1/2⟨111⟩ loops during the shock wave compression in the [111] Mo crystal at 500 ms^{-1} and 300 K at (a) 58, (b) 66, and (c) 70 ps. Purple and green lines represent ⟨100⟩ and 1/2⟨111⟩ dislocation segments, respectively. Arrows show the direction of Burgers vector.

stress τ of about 10–20 GPa. Therefore, when the main mechanism of plastic deformation is the activation of the screw dislocations from the dislocation loops, the shear stress relaxation is expected to decrease over some distance traveled by the shock wave. This can lead to a slowing of the elastic precursor decay.

F. [100] Mo crystal with dislocations

In the [100] molybdenum crystal with dislocations, the multiplication of screw dislocations behind the wave front is also observed as in the case of other Mo crystals [Figs. 12(c)–12(d)]. The formation of an elastic precursor is observed at 500 ms^{-1} already in Fig. 12(a); however, it is much slower than for other crystal orientations. It can be seen that the stress at precursor almost does not change at 500 ms^{-1} throughout the shock wave propagation. The shear stress τ_{100} at the top of elastic precursor is also close to that in the [110] and [111] Mo crystals.

Behind the shock wave front, the formation of twin bands is observed at 900 ms^{-1} in Fig. 12(d). The direction of these bands coincides with dislocation loops that propagate from the existing edge dislocation segments. The shear stress decays monotonically behind the wave front in this case [Fig. 12(b)], which means that the growth of twin bands activated at some temperature is a more intense plastic deformation process through which an elastic precursor may be formed.

The presence of a single wave configuration without the formation of an elastic precursor in [100] crystals is known for fcc metals, such as copper.[64,65] However, in the fcc crystals, it is due to the low value of the shear modulus along the axis [100] because of which the longitudinal and bulk wave velocities are close to each other. In the [100] Mo crystal, the shear stresses τ of around 10–25 GPa are found behind the shock front at 500–900 ms^{-1} [Figs. 12(a) and 12(b)], which are sufficient to activate the dislocation multiplication, resulting in the formation of elastic precursor.

G. Elastic precursor decay

The elastic precursor decay in [110], [111] Mo crystals at 500 and 900 ms^{-1} is shown in Fig. 13. The HEL stress, σ_{xx}, decreases initially due to thermal softening and, in most cases, subsequently decays with nearly identical slopes across all temperatures. This leads to a lower HEL value with increasing temperature throughout the shock wave propagation. Figure 13 shows a decrease in HEL values with temperature for the Mo crystal orientations and particle velocities considered in the study. It can be observed that the temperature dependence of HEL shows little variation with crystal orientation when the shock wave propagates a distance of 600 to 850 nm.

The HEL initially decays differently in the region where it forms, but after approximately 100–300 nm shock propagation, the decay transitions to a consistent slope. This behavior was observed earlier for the copper crystals.[27] In this region, the HEL decay is well approximated by the power law function,

$$\sigma_{\mathrm{HEL}} = \sigma_0 (x/x_0)^{-\alpha}, \tag{5}$$

where α is a HEL decay exponent and x_0 is equal to 1 nm. The approximation is only valid in the region of consistent slope. The σ_0 parameter does not represent the maximum HEL stress and may exceed the initial stress in the shock wave.

The decay exponent α clearly depends on crystal orientation, but it is almost independent of temperature. The decay exponent falls within the range of 0.25–0.45. For example, at 500 ms^{-1}, the decay exponent is approximately 0.45 and 0.30 for [110] and [111] Mo crystals. The HEL decay for the [110] crystal becomes lower than that for the [111] crystal at 900 ms^{-1}, which is probably due to the faster formation of the elastic precursor at the early stage of shock propagation. The obtained range of decay exponents due to multiplication of preexisting dislocation in Mo crystal is confirmed by a series of atomistic simulations using Ackland's potential (Figs. S1, S2 in the supplementary material).

At 500 ms^{-1}, the HEL values at the end of shock propagation are higher for the [111] orientation, ranging from 24 to 27 GPa, compared to the [110] orientation, which ranges from 19 to 22 GPa, depending on temperature [Figs. 13(a) and 13(b)]. When the particle velocity increases to 900 ms^{-1}, the HEL values for [111] and

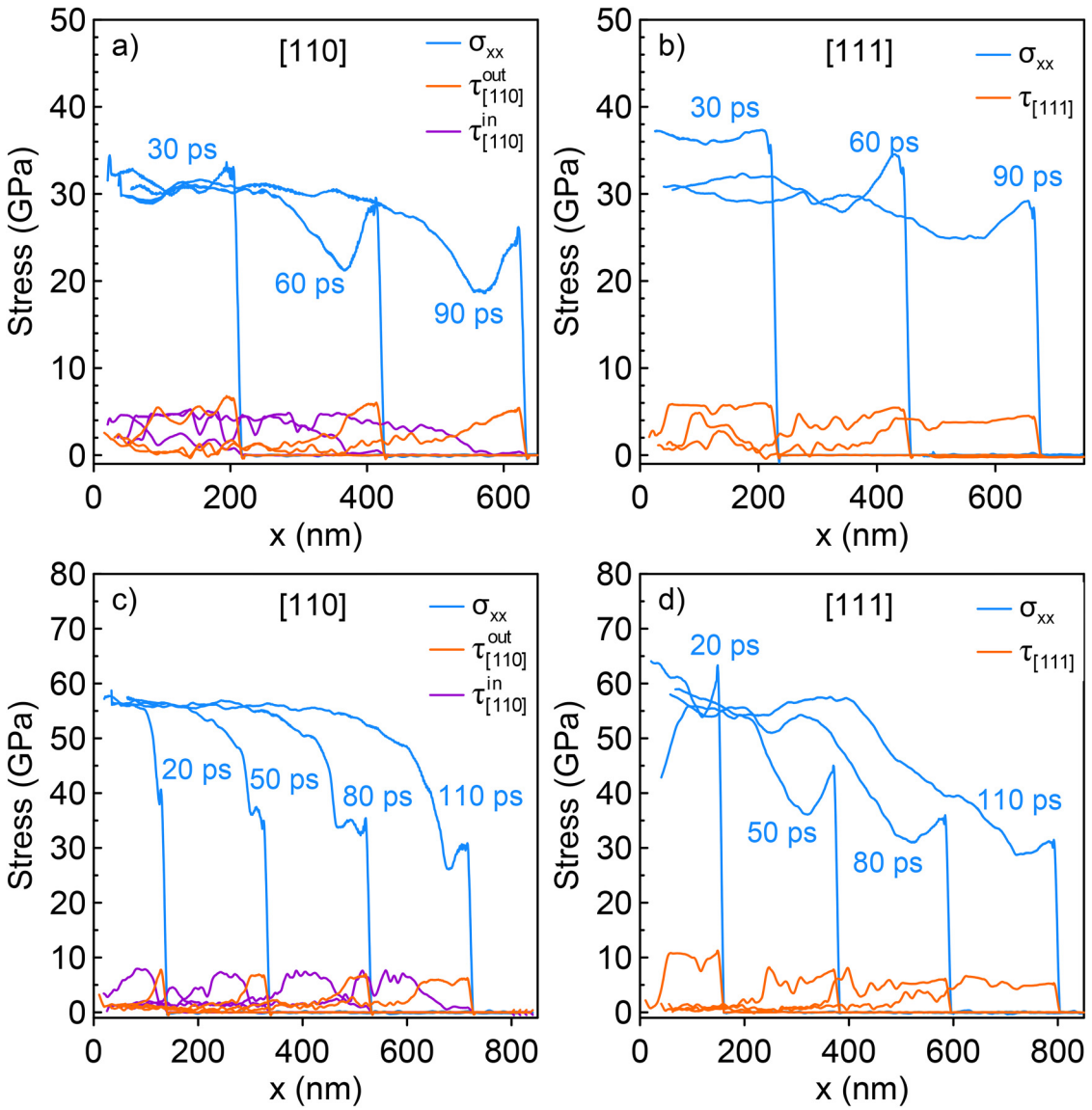

FIG. 11. Longitudinal σ_{xx} and resolved shear stress τ at ⟨111⟩ {110} slip systems in (a,c) [110] and (b,d) [111] Mo crystals with preexisting dislocations at (a,b) 300 K and 500 ms^{-1} and (c,d) 700 K and 900 ms^{-1}. The dislocation evolution in (a) and (b) is shown in Figs. 6 and 7, respectively.

[110] crystals become close, ranging from 25 to 30 GPa [Figs. 13(c) and 13(d)].

The elastic precursor decay in the [100] Mo crystal is shown in Fig. 14. The case of the [100] crystal is specific, as the elastic precursor forms very slowly and decays only slightly. Due to its slower decay, the HEL for the [100] Mo crystal exhibits higher values than for [110] and [111] crystals at certain shock propagation distances (Fig. 13). The decay exponent in [100] Mo crystal is close to 0.10 at 500 ms^{-1} [Fig. 14(a)]. The decay exponent starts to increase to 0.3–0.4 only at 900 ms^{-1} when temperature is above 1600 K [Fig. 14(c)]. In that range, the twinning is activated behind the shock wave front (Fig. 12). The post-spike minimum decreases with propagation distance, while the spike values remain relatively unchanged [Figs. 14(a) and 14(b)]. The decay exponent of the post-spike minimum is in the range of 0.2–0.3, which is close to the values observed for [110] and [111] crystals in Fig. 5.

These observations are quite similar to those reported in experiments on pristine [100] Mo crystals.[10,23] The HEL at spike varies slowly with decay exponent less than 0.1 when the shock

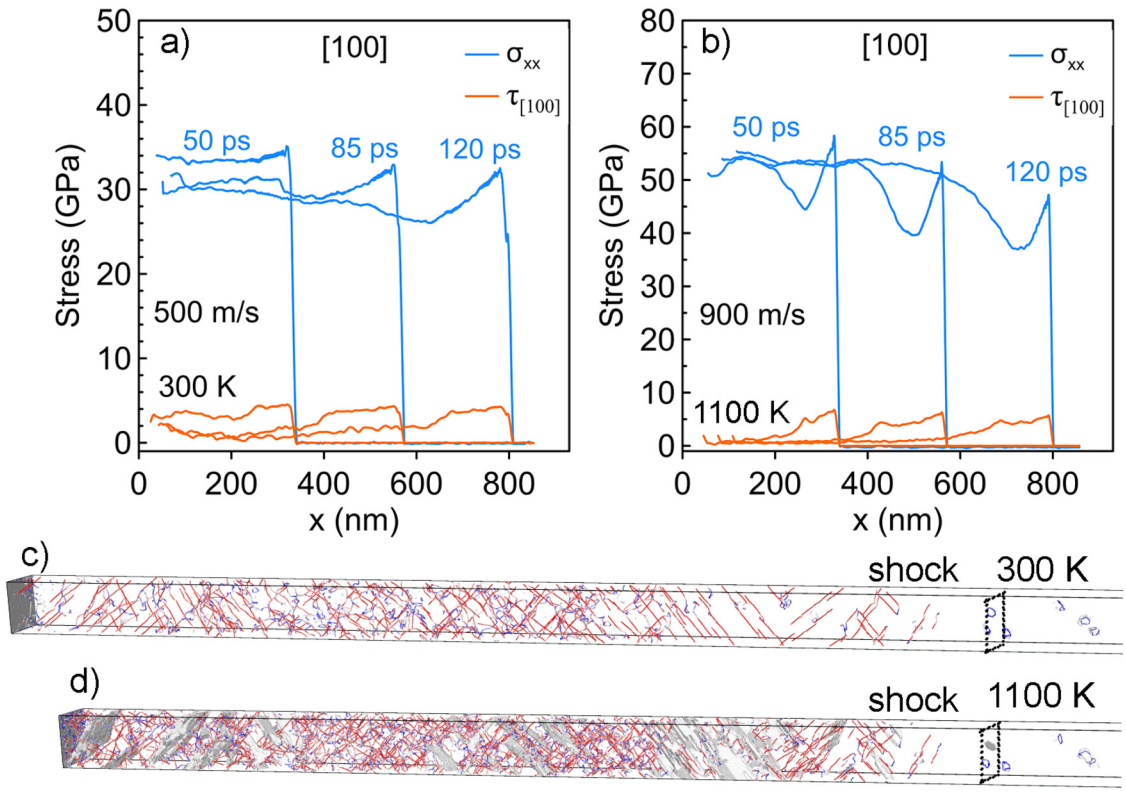

FIG. 12. Longitudinal σ_{xx} and resolved shear stress $\tau_{[100]}$ at $\langle 111 \rangle$ {110} slip systems in [100] Mo crystals with preexisting dislocations at (a) 300 and (b) 1100 K at 500 and 900 ms^{-1}, respectively. Dislocation substructure at (c) 300 and (d) 1100 K at 85 ps, corresponding to the shock profiles in (a) and (b), respectively. Red and blue lines correspond to screw and edge dislocation segments. Gray region represents the defective region produced by the dislocation extraction algorithm.[63]

propagates the distance between 0.2 and 8 mm. Plastic relaxation, driven by the multiplication of dislocations, takes place behind the spike, resulting in a decrease in the post-spike minimum with increasing propagation distance[10] with a decay exponent of 0.36. The decay exponent for 0.6% and 5.4% pre-strained [100] Mo crystals is between 0.15 and 0.36, respectively.

The spiked shape of the elastic precursor actually is observed for all crystal orientation at 500 ms^{-1} (Figs. 11 and 12). The spike usually forms when plastic deformation processes are intense, leading to local stress relaxation behind the shock wave front. The front part of the wave is initially unaware of this relaxation, and it takes time for the rarefaction wave to propagate and reduce the stress at the shock front.[27] Sometimes, when plastic deformation occurs very rapidly, as in the case of dislocation nucleation, the spike shape is maintained because the rarefaction wave cannot reach the peak of the shock wave.[66] In our simulations, the dislocations activity begins only some distance away from the front part of the elastic precursor, and the dislocation density does not increase at the top [Figs. 6, 7, 12(c), 12(d), and S4]. Thus, the slower HEL decay at the spike in the [100] crystal, compared to other crystals, may be related to the slower speed of sound along the [100] direction, which is known for cubic crystals. The slower the rarefaction wave propagates from the relaxed region to the peak, the slower the HEL will decay.

In shock compression experiments for annealed Mo,[9,10] the elastic precursor decay has two stages. In the first stage, up to 0.2 mm, the HEL decay exponent is around 0.6–0.7 and is independent of temperature.[9,10] The shear stress corresponding to the precursor spike decreases very fast during this stage, from 3.4 GPa to approximately 1.2 GPa in the [100] Mo crystal shocked at compressive stress of 12.5 GPa.[10,23] The HEL values weakly decrease with temperature.[9] Only in the next stage, after 0.2 mm of shock propagation, the HEL decay begins to depend on temperature more strongly, with the HEL value decreasing markedly with temperature for polycrystalline Mo.[9]

Our results in Figs. 13 and 14 show that at a distance of about 1 μm, the HEL values weakly decreases with temperature when the main mechanism of plastic deformation is multiplication of dislocation loops. It is noteworthy that in other bcc metals, such as Nb, Cr, and W, the HEL decreases significantly with temperature even in the first stage of HEL decay.[9,11]

The elastic precursor decay exponents for Mo crystals obtained in the range of 0.25–0.45 in our simulations are lower than the values of 0.8–1.0 at the first stage of elastic decay.[9,10] This means that

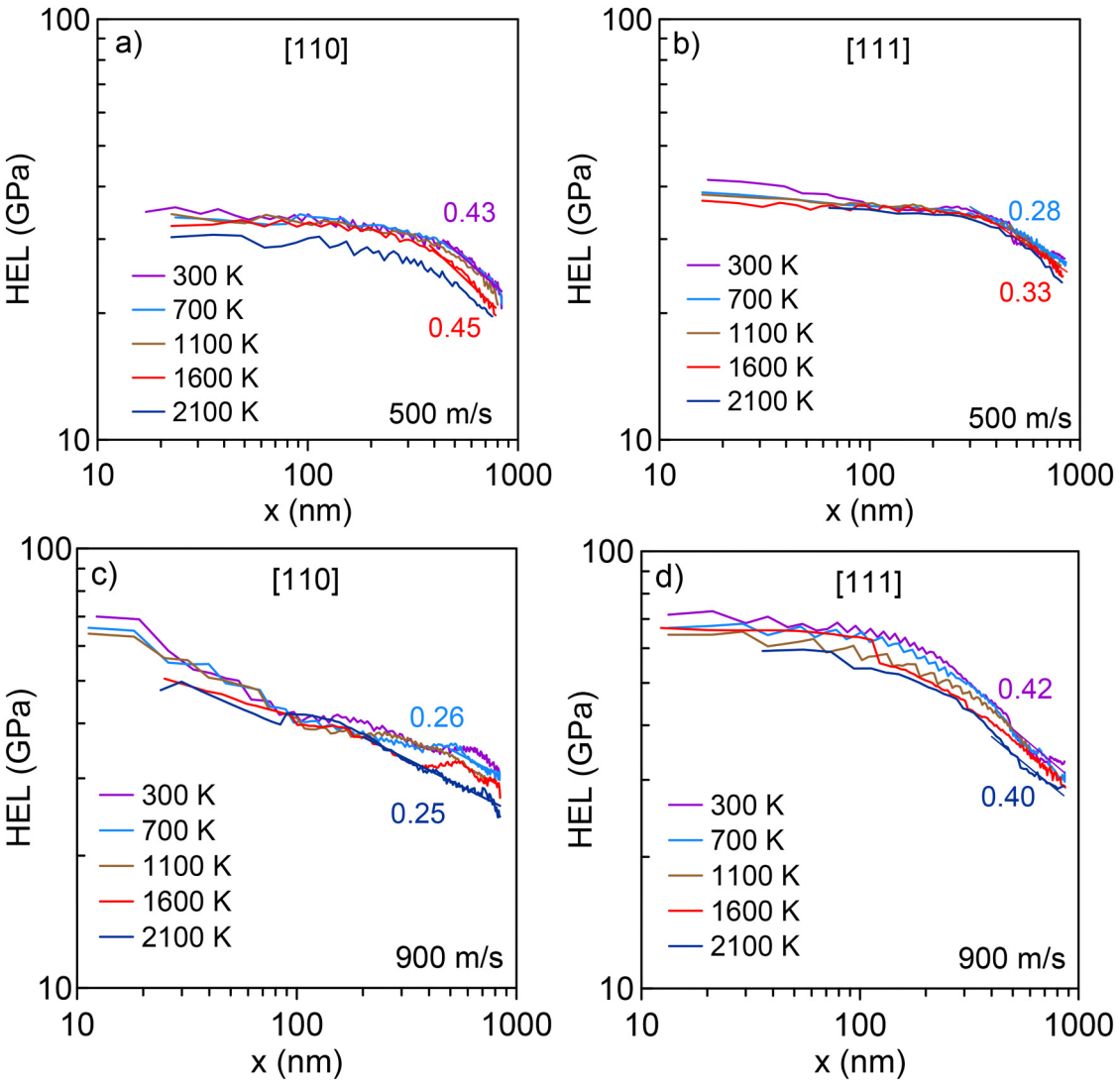

FIG. 13. Temperature dependence of longitudinal stress σ_{xx} at elastic precursor (GPa) in (a) and (c) [110] and (b) and (d) [111] Mo crystals with dislocation at a particle velocity of (a) and (b) 500 and (c) and (d) 900 ms^{-1}. The figures are shown in logarithmic scale. The numbers show the decay exponent [Eq. (5)], and the color indicates the temperature to which it applies.

the mechanism of multiplication of screw dislocation from preexisting dislocation loops is rather slow, and there should be a faster mechanism of plastic deformation when the shock propagation distance is below 0.2 mm. However, the obtained range of decay exponents agrees well with the experimental values of 0.2–0.4 for polycrystalline Mo and pre-strained [100] Mo crystals in the second stage.[9,11] Such an agreement indicates that at this stage plastic deformation behind the shock wave front is provided by dislocation multiplication. Moreover, same mechanisms also occur in [100] crystals, where a clear spike and post-spike minimum in the shock wave structure are observed.

A possible reason why we do not observe a faster mechanism of plastic deformation, possibly twinning with an exponent of 0.8–1.0, is likely related to the high dislocation density in our models, which hinders the formation of twins. It is worth noting that, apparently, in molybdenum samples that have not been annealed or have been pre-deformed, twinning also does not occur, as indicated by the exponent of 0.2–0.4. Therefore, it is likely that the particle velocities at which twinning can be observed in our models must exceed 900 ms^{-1}, although this is still higher than the particle velocities observed in experiments during the first stage.

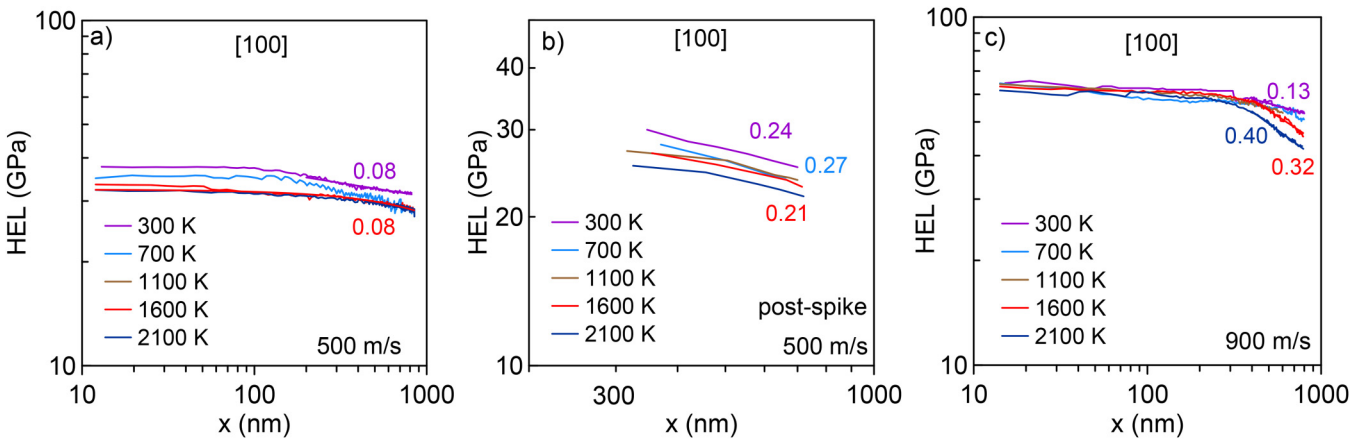

FIG. 14. Temperature dependence of HEL stress σ_{xx} (GPa) as a function of shock propagation distance in [100] Mo crystals with dislocations. The (a) spike and (b) post-spike values for particle velocity of 500 ms^{-1} and (c) HEL at spike at 900 ms^{-1}. The figures are shown in the logarithmic scale. The numbers show the decay exponent [Eq. (5)], and the color indicates the temperature to which it applies.

IV. SUMMARY

The response of bcc Mo crystals of different orientation with and without preexisting dislocation substructure to shock compression is studied using molecular dynamic simulations. An attempt has been made to analyze the evolution of dislocations from the preexisting dislocations behind the shock wave in bcc crystals. With this aim, the atomic models of [100], [110], and [111] Mo crystals with the density of $1/2\langle 111\rangle$ and $\langle 100\rangle$ preexisting dislocations loops are constructed having the length of almost 1 μm along the shock direction.

The simulations indicate that the primary mechanism of plastic deformation behind the shock wave is the multiplication of dislocation loops originating from preexisting dislocations. Before expansion, the $1/2\langle 111\rangle$ loops undergo a rotation, aligning to the plane orthogonal to their Burgers vector. In contrast, the $\langle 100\rangle$ loops act as sources for screw dislocation segments. These segments propagate both forward and backward relative to the shock wave direction, leading to the formation of dislocation loops. The growth of dislocation loops occurs primarily through the motion of screw dislocation segments. With increasing temperature and particle velocity in the shock wave, the formation of twin bands is observed in the [110] and [100] crystals but not in [111] Mo crystals.

The elastic precursor forms in the shock wave structure in [100], [110], and [111] Mo crystals with dislocations at 500 ms^{-1} and then decays. In [100] Mo crystals, the elastic precursor forms and decays much more slowly than in other crystals. However, the post-spike HEL values decay with the same exponents as in other crystals.

The decay of elastic precursor is found almost independent of temperature at 500 and 900 ms^{-1}. The HEL values decrease with increasing temperature in Mo crystals during shock wave propagation. However, in most cases, the HEL decreases by less than 20% with an increase in temperature from 300 to 2100 K. These results are in qualitative agreement with experiments.[9] The HEL decay exponent of the elastic precursor in the calculations is in the range of 0.25–0.45, which is in agreement with the HEL decay when the shock travels no less than 0.2 mm. The higher HEL decay exponent of 0.6–0.7 at shock propagation distance beyond 0.2 mm suggests that there exists a faster plastic deformation process behind the wave front than the multiplication of preexisting dislocation loops at early stages.

In perfect Mo crystals, the shock wave structure consists of defect-free elastic precursor and plastic shock wave in which the plastic deformation occurs. The plastic deformation is attained by the nucleation of dislocation in front of plastic wave and their subsequent multiplication. The elastic precursor has the plateau shape at moderate particle velocities, but some perturbations of its structure are found when the particle velocity increases. After formation, the HEL attenuates to some value and then almost does not change and decay. The HEL values are found to be higher in [111] crystals compared to [110] Mo perfect crystals. While the HEL decreases with temperature for the [111] crystal, it remains almost temperature-independent for the [110] crystal.

The simulation results agree with experimental observations regarding the temperature dependence of the HEL. They also reproduce higher HEL values for [111] Mo crystals compared to [110] crystals,[23] both in the presence of dislocation loops and without them. The present paper is perhaps the one of the first attempts to study the shock structure for bcc crystals with the dislocations at a distances close to 1 μm over a wide temperature range. It would be interesting to study in future the plastic deformation mechanisms of HEL decay during the initial stages of shock wave propagation in Mo crystals.

SUPPLEMENTARY MATERIAL

See the supplementary material for the decay of the stress at elastic precursor obtained using Ackland's potential[57] for Mo,

along with the evolution of unidentified loops and the dislocation density behind the shock wave.

ACKNOWLEDGMENTS

The research was carried out using the equipment of the shared research facilities of HPC computing resources and the MSU-270 supercomputer at Lomonosov Moscow State University.[67] The reported study is supported by the Russian Science Foundation (RSF), Research Project No. 22-71-00088.

AUTHOR DECLARATIONS

Conflict of Interest

The authors have no conflicts to disclose.

Author Contributions

I. A. Bryukhanov: Conceptualization (equal); Data curation (equal); Formal analysis (equal); Investigation (equal); Methodology (equal); Software (equal); Supervision (equal); Writing – original draft (equal); Writing – review & editing (equal). **E. V. Fomin:** Methodology (equal); Validation (equal); Writing – review & editing (equal).

DATA AVAILABILITY

The data that support the findings of this study are available from the corresponding author upon reasonable request.

REFERENCES

[1]Y. B. Zel'dovich and Y. P. Raizer, *Physics of Shock Waves and High-Temperature Hydrodynamic Phenomena* (Academic Press, New York, 1966).
[2]M. A. Meyers and L. E. Murr, *Shock Waves and High-Strain-Rate Phenomena in Metals* (Springer US, Boston, 1981).
[3]C. Montross, "Laser shock processing and its effects on microstructure and properties of metal alloys: A review," Int. J. Fatigue **24**(10), 1021–1036 (2002).
[4]G. I. Kanel, S. V. Razorenov, and V. E. Fortov, *Shock-Wave Phenomena and the Properties of Condensed Matter* (Springer Science and Business Media, 2004).
[5]E. B. Zaretsky and G. I. Kanel, "Abnormal temperature effects on the dynamic yield stress of alpha-brass," J. Appl. Phys. **124**(4), 045902 (2018).
[6]E. B. Zaretsky, N. Frage, and S. Kalabukhov, "Shock wave determination of the strengthening of commercial aluminum alloy 6061 by point defects," Mater. Sci. Eng. A **761**, 138066 (2019).
[7]E. B. Zaretsky and G. I. Kanel, "Yield stress, polymorphic transformation, and spall fracture of shock-loaded iron in various structural states and at various temperatures," J. Appl. Phys. **117**(19), 195901 (2015).
[8]E. B. Zaretsky and G. I. Kanel, "Tantalum and vanadium response to shock-wave loading at normal and elevated temperatures. Non-monotonous decay of the elastic wave in vanadium," J. Appl. Phys. **115**(24), 243502 (2014).
[9]E. B. Zaretsky and G. I. Kanel, "Invariability of rate dependences of normalized flow stress in niobium and molybdenum under conditions of shock compression," J. Appl. Phys. **120**(10), 105901 (2016).
[10]G. I. Kanel, G. V. Garkushin, A. S. Savinykh, S. V. Razorenov, I. V. Paramonova, and E. B. Zaretsky, "Effect of small pre-strain on the resistance of molybdenum [100] single crystal to high strain rate deformation and fracture," J. Appl. Phys. **131**(9), 095903 (2022).
[11]E. B. Zaretsky and G. I. Kanel, "The high temperature impact response of tungsten and chromium," J. Appl. Phys. **122**(11), 115901 (2017).
[12]I. A. Bryukhanov and D. Chaikovskii, "Role of solid solution strengthening on shock wave compression of [111] copper crystals," J. Appl. Phys. **135**(22), 225902 (2024).
[13]E. B. Zaretsky and G. I. Kanel, "Effect of temperature, strain, and strain rate on the flow stress of aluminum under shock-wave compression," J. Appl. Phys. **112**(7), 073504 (2012).
[14]E. B. Zaretsky and G. I. Kanel, "Response of copper to shock-wave loading at temperatures up to the melting point," J. Appl. Phys. **114**(8), 083511 (2013).
[15]J. Chang, W. Cai, V. V. Bulatov, and S. Yip, "Dislocation motion in BCC metals by molecular dynamics," Mater. Sci. Eng. A **309–310**, 160–163 (2001).
[16]N. R. Barton, J. V. Bernier, R. Becker, A. Arsenlis, R. Cavallo, J. Marian, M. Rhee, H.-S. Park, B. A. Remington, and R. T. Olson, "A multiscale strength model for extreme loading conditions," J. Appl. Phys. **109**(7), 073501 (2011).
[17]A. Y. Kuksin and A. V. Yanilkin, "Atomistic simulation of the motion of dislocations in metals under phonon drag conditions," Phys. Solid State **55**(5), 1010–1019 (2013).
[18]S. Starikov and V. Tseplyaev, "Two-scale simulation of plasticity in molybdenum: Combination of atomistic simulation and dislocation dynamics with nonlinear mobility function," Comput. Mater. Sci. **179**, 109585 (2020).
[19]M. R. Gilbert, S. Queyreau, and J. Marian, "Stress and temperature dependence of screw dislocation mobility in α-Fe by molecular dynamics," Phys. Rev. B **84**(17), 174103 (2011).
[20]S. Yao, X. Pei, Z. Liu, J. Yu, Y. Yu, and Q. Wu, "Numerical investigation of the temperature dependence of dynamic yield stress of typical BCC metals under shock loading with a dislocation-based constitutive model," Mech. Mater. **140**, 103211 (2020).
[21]G. I. Kanel, S. V. Razorenov, A. V. Utkin, V. E. Fortov, K. Baumung, H. U. Karow, D. Rusch, and V. Licht, "Spall strength of molybdenum single crystals," J. Appl. Phys. **74**(12), 7162–7165 (1993).
[22]A. Mandal and Y. M. Gupta, "Elastic-plastic deformation of molybdenum single crystals shocked along [100]," J. Appl. Phys. **121**(4), 045903 (2017).
[23]A. Mandal and Y. M. Gupta, "Elastic-plastic deformation of molybdenum single crystals shocked to 12.5 GPa: Crystal anisotropy effects," J. Appl. Phys. **125**(5), 055903 (2019).
[24]T. Oniyama, Y. M. Gupta, and G. Ravichandran, "Shock compression of molybdenum single crystals to 110 GPa: Elastic–plastic deformation and crystal anisotropy," J. Appl. Phys. **127**(20), 205902 (2020).
[25]T. Oniyama, Y. M. Gupta, and G. Ravichandran, "Peak states of molybdenum single crystals shock compressed to high stresses," J. Appl. Phys. **129**(24), 245906 (2021).
[26]V. Gandhi, S. Ravindran, A. Joshi, and G. Ravichandran, "Real-time characterization of dislocation slip and twinning of shock-compressed molybdenum single crystals," Phys. Rev. Mater. **7**(7), 073601 (2023).
[27]I. A. Bryukhanov, "Role of temperature and preexisting dislocation network on the shock compression of copper crystals," Int. J. Plast. **165**, 103599 (2023).
[28]V. V. Zhakhovsky, M. M. Budzevich, N. A. Inogamov, I. I. Oleynik, and C. T. White, "Two-zone elastic-plastic single shock waves in solids," Phys. Rev. Lett. **107**(13), 135502 (2011).
[29]V. V. Zhakhovsky, N. A. Inogamov, B. J. Demaske, I. I. Oleynik, and C. T. White, "Elastic-plastic collapse of super-elastic shock waves in face-centered-cubic solids," J. Phys.: Conf. Ser. **500**(17), 172007 (2014).
[30]R. Perriot, V. V. Zhakhovsky, N. A. Inogamov, and I. I. Oleynik, "Evolution of elastic precursor and plastic shock wave in copper via molecular dynamics simulations," J. Phys.: Conf. Ser. **500**(17), 172008 (2014).
[31]R. Ravelo, T. C. Germann, O. Guerrero, Q. An, and B. L. Holian, "Shock-induced plasticity in tantalum single crystals: Interatomic potentials and large-scale molecular-dynamics simulations," Phys. Rev. B **88**(13), 134101 (2013).
[32]D. Tramontina, P. Erhart, T. Germann, J. Hawreliak, A. Higginbotham, N. Park, R. Ravelo, A. Stukowski, M. Suggit, Y. Tang, J. Wark, and E. Bringa, "Molecular dynamics simulations of shock-induced plasticity in tantalum," High Energy Density Phys. **10**, 9–15 (2014).

[33]D. Wu, K. Chen, Y. Zhu, L. Zhao, M. Huang, and Z. Li, "Unveiling grain size effect on shock-induced plasticity and its underlying mechanisms in nano-polycrystalline Ta," Mech. Mater. **160**, 103952 (2021).
[34]S. Galitskiy, A. Mishra, and A. M. Dongare, "Modeling shock-induced void collapse in single-crystal Ta systems at the mesoscales," Int. J. Plast. **164**, 103596 (2023).
[35]R. Kositski, D. Steinberger, S. Sandfeld, and D. Mordehai, "Shear relaxation behind the shock front in ⟨110⟩ molybdenum – from the atomic scale to continuous dislocation fields," Comput. Mater. Sci. **149**, 125–133 (2018).
[36]Y. Hu, S. Ding, J. Xu, Y. Zhang, W. Wu, and R. Xia, "Anisotropic orientation dependent shock wave responses of monocrystalline molybdenum," J. Mater. Res. Technol. **25**, 285–296 (2023).
[37]S. J. Wang, H. Wang, K. Du, W. Zhang, M. L. Sui, and S. X. Mao, "Deformation-induced structural transition in body-centred cubic molybdenum," Nat. Commun. **5**(1), 3433 (2014).
[38]S. Mahajan and A. F. Bartlett, "Influence of prior mechanical and thermal treatments on shock-induced substructures in molybdenum," Acta Metall. **19**(10), 1111–1119 (1971).
[39]K. Wongwiwat and L. E. Murr, "Effect of shock pressure, pulse duration, and grain size on shock-deformation twinning in molybdenum," Mater. Sci. Eng. **35**(2), 273–285 (1978).
[40]L. A. Zepeda-Ruiz, A. Stukowski, T. Oppelstrup, and V. V. Bulatov, "Probing the limits of metal plasticity with molecular dynamics simulations," Nature **550**(7677), 492–495 (2017).
[41]L. A. Zepeda-Ruiz, A. Stukowski, T. Oppelstrup, N. Bertin, N. R. Barton, R. Freitas, and V. V. Bulatov, "Atomistic insights into metal hardening," Nat. Mater. **20**(3), 315–320 (2021).
[42]I. A. Bryukhanov and V. A. Emelyanov, "Shear stress relaxation through the motion of edge dislocations in Cu and Cu–Ni solid solution: A molecular dynamics and discrete dislocation study," Comput. Mater. Sci. **201**, 110885 (2022).
[43]I. A. Bryukhanov, "Atomistic simulation of the shock wave in copper single crystals with pre-existing dislocation network," Int. J. Plast. **151**, 103171 (2022).
[44]T. D. Swinburne, "Coarse-graining and forecasting atomic material simulations with descriptors," Phys. Rev. Lett. **131**(23), 236101 (2023).
[45]A. E. Mayer, "Influence of preliminary compressive deformation on the spall strength of aluminum single crystal," Scr. Mater. **242**, 115905 (2024).
[46]J. C. Stimac, N. Bertin, J. K. Mason, and V. V. Bulatov, "Energy storage under high-rate compression of single crystal tantalum," Acta Mater. **239**, 118253 (2022).
[47]N. Bertin, R. Carson, V. V. Bulatov, J. Lind, and M. Nelms, "Crystal plasticity model of BCC metals from large-scale MD simulations," Acta Mater. **260**, 119336 (2023).
[48]B. D. Wirth, G. R. Odette, D. Maroudas, and G. E. Lucas, "Dislocation loop structure, energy and mobility of self-interstitial atom clusters in bcc iron," J. Nucl. Mater. **276**(1–3), 33–40 (2000).
[49]M. A. Puigvi, Y. N. Osetsky, and A. Serra, "Point-defect clusters and dislocation loops in bcc metals: Continuum and atomistic study," Philos. Mag. **83**(7), 857–871 (2003).
[50]J. Fikar, R. Schäublin, D. R. Mason, and D. Nguyen-Manh, "Nano-sized prismatic vacancy dislocation loops and vacancy clusters in tungsten," Nucl. Mater. Energy **16**, 60–65 (2018).
[51]A. Stukowski, V. V. Bulatov, and A. Arsenlis, "Automated identification and indexing of dislocations in crystal interfaces," Modell. Simul. Mater. Sci. Eng. **20**(8), 085007 (2012).
[52]A. Stukowski, "Computational analysis methods in atomistic modeling of crystals," JOM **66**(3), 399–407 (2014).
[53]A. Stukowski, "Visualization and analysis of atomistic simulation data with OVITO—the open visualization tool," Modell. Simul. Mater. Sci. Eng. **18**(1), 015012 (2010).
[54]X. W. Zhou, R. A. Johnson, and H. N. G. Wadley, "Misfit-energy-increasing dislocations in vapor-deposited CoFe/NiFe multilayers," Phys. Rev. B **69**(14), 144113 (2004).
[55]S. Plimpton, "Fast parallel algorithms for short-range molecular dynamics," J. Comput. Phys. **117**(1), 1–19 (1995).
[56]H. Carter Edwards, C. R. Trott, and D. Sunderland, "Kokkos: Enabling many core performance portability through polymorphic memory access patterns," J. Parallel Distrib. Comput. **74**(12), 3202–3216 (2014).
[57]G. J. Ackland and R. Thetford, "An improved N -body semi-empirical model for body-centred cubic transition metals," Philos. Mag. A **56**(1), 15–30 (1987).
[58]S. Starikov, P. Grigorev, and P. A. T. Olsson, "Angular-dependent interatomic potential for large-scale atomistic simulation of W-Mo-Nb ternary alloys," Comput. Mater. Sci. **233**, 112734 (2024).
[59]J. M. Dickinson and P. E. Armstrong, "Temperature dependence of the elastic constants of molybdenum," J. Appl. Phys. **38**(2), 602–606 (1967).
[60]F. H. Featherston and J. R. Neighbours, "Elastic constants of tantalum, tungsten, and molybdenum," Phys. Rev. **130**(4), 1324–1333 (1963).
[61]W. Luo, D. Roundy, M. L. Cohen, and J. W. Morris, "Ideal strength of bcc molybdenum and niobium," Phys. Rev. B **66**(9), 094110 (2002).
[62]H. Bei, Y. F. Gao, S. Shim, E. P. George, and G. M. Pharr, "Strength differences arising from homogeneous versus heterogeneous dislocation nucleation," Phys. Rev. B **77**(6), 060103 (2008).
[63]A. Stukowski and A. Arsenlis, "On the elastic–plastic decomposition of crystal deformation at the atomic scale," Modell. Simul. Mater. Sci. Eng. **20**(3), 035012 (2012).
[64]E. M. Bringa, J. U. Cazamias, P. Erhart, J. Stölken, N. Tanushev, B. D. Wirth, R. E. Rudd, and M. J. Caturla, "Atomistic shock Hugoniot simulation of single-crystal copper," J. Appl. Phys. **96**(7), 3793–3799 (2004).
[65]A. Neogi and N. Mitra, "Evolution of dislocation mechanisms in single-crystal Cu under shock loading in different directions," Modell. Simul. Mater. Sci. Eng. **25**(2), 025013 (2017).
[66]R. Kositski and D. Mordehai, "On the origin of the stress spike decay in the elastic precursor in shocked metals," J. Appl. Phys. **126**(8), 085901 (2019).
[67]V. Sadovnichy, A. Tikhonravov, V. Voevodin, and V. Opanasenko, "Lomonosov: Supercomputing at Moscow State University," in *Contemporary High Performance Computing: From Petascale Toward Exascale*, edited by J. S. Vetter (CRC Press, Boca Raton, 2013), pp. 283–307.